Characterization of the laser-ablation plasmas using optical spectroscopy and opto-acoustic methods

C. NEGUTU, M. STAFE, S. S. CIOBANU, N. N. PUSCAS*
University "Politehnica" of Bucharest, Physics Department, Splaiul Independentei 313, 060042, Bucharest, Romania,

This paper presents an experimental spectroscopic study of the laser-ablation plasmas generated on different solid targets (Al, Cu and Er^{3+}-doped Ti:$LiNbO_3$) under room conditions. We analysed the visible spectrum in order to evaluate the peak temperature and the spatial variation of the temperature within the ablation plasma plume along the axial direction by scanning axially the plume image with a fiber tip that is coupled at a spectrometer entrance. The results indicate that the intensity of the lines increases when increasing the distance from the ablated target surface, while the plasma temperature calculated by accounting for these lines intensities is almost constant, non-dependent on the laser-irradiance and the distance from the target in the experimental conditions that we used. The laser-ablation plasmas and the generated shock waves in multi-pulse regime were further characterized by using an opto-acoustic method. Opto-acoustics allows for studying both the thermal and optical effects induced by the laser radiation, such as the changes in the dimensions of the ablated structure, ablation rate and the dynamics of the ablation products (plasma). The thermal effects such as those involved in laser ablation (e.g. melting, recrystallization) were additionally addressed by coupling time resolved reflectivity (TRR) and rapid infrared pyrometry (RIP) under atmospheric pressure hemispherical reactor. The changes of surface morphology caused by melting and recrystallization during soft or hard ablation are discussed. The dependences of the electrical conductivity on time and temperature and of the effusivity on time for Au/Ni/Bronze coating are also analysed.

(Received February 14, 2011; accepted July 25, 2011)

Keywords: Laser plasma spectroscopy, Time resolved reflectivity, Rapid infrared pyrometry, Opto-acoustics

1. Introduction

In the last years, several experimental and theoretical studies were achieved concerning laser processing at nanosecond scale, mainly on temperature and surface-morphology dependence of the thermal and optical properties of the targets that are subjected to laser radiation [1, 2]. The optical methods which were used in these studies are precise and powerful because in many cases they are nondestructive, simple, sensitive, and have high temporal/spatial resolution [3-7].

Plasma formation during irradiation of solids with intense laser pulses is the subject of investigations in many fields of applied and fundamental research, from laser-plasma sources to X-ray lasers, from inertial confinement fusion to laboratory astrophysics. We used the emission spectroscopy of Al, Cu and Er^{3+}-doped Ti:$LiNbO_3$ plasmas in air generated by the second harmonic of a Q-switched Nd-YAG laser. The space variation of intensities for different spectral lines along the axial direction within the plasma plume was measured by scanning axially the plume image with a fiber that is coupled at a spectrometer entrance slit. Then the temperature was evaluated using a Boltzmann plot. An opto-dynamic approach is additionally presented here in order to study the thermal and optical effects induced by the laser radiation, such as the dynamics of the ablation products, ablation plasma, and the generation of shock waves during laser processing of a material.

The phase and/or structural changes induced on the target, by the laser radiation, are detected by means of the time-resolved reflectivity (TRR) method [5-7]. This optical method was earlier used to investigate semi-conductor materials and thin films properties during pulsed laser processing [5-7]. The pulsed laser heats the sample and induces temperature rise, phase, morphological or other changes on its surface. A low power CW laser probes those changes simultaneously with heating. The simplicity of the method enables the use of TRR method in many and various applications, from the in-situ monitoring of the phase changes to proving of mathematical models. Thus, optical (reflectivity, absorption coefficient, refraction index, etc.) and electrical (conductivity, dielectric constants, etc.) properties were obtained from reflectivity data and were used for the characterization of the materials. The huge variation of reflectivity from solid to liquid phase (i. e. from 35 % to 73 % in the case of typically crystalline silicon) allows achieving high quality measurements. This is not the case with pure metals and ceramics, where the reflectivity changes from solid to liquid phase are less than 10 %.

In order to investigate the thermal changes, direct temperature measurement is proposed by rapid infrared pyrometry (RIP) systems [5-7]. The coupling of the two methods (RIP and TRR) allows the study of the melting kinetics induced by laser radiation in a large number of bulk metallic, dielectric and semi-conductor materials [5-7], and of the new phenomena induced by UV pulsed lasers, such as thin film melting kinetics, liquid phase

segregation, soft ablation and finally plasma expansion. Also, the changes of surface morphology caused by melting and recrystallization during soft or hard ablation were discussed [6].

The paper is organized as follows. In Section 2 the laser-ablation plasmas generated on Al, Cu and Er^{3+}-doped Ti:$LiNbO_3$ targets in atmospheric air under room conditions are analysed using optical emission spectroscopy. Section 3 is devoted to the opto-acoustic analysis of the laser ablation. In the case of Au/Ni/Bronze system, the TRR and PIR methods used to study phase transitions on the target surface during and after the KrF laser irradiation are presented in Section 4, while Section 5 is devoted to the conclusions.

2. Characterization of the laser-ablation plasmas by optical methods

The experimental setup used for the spectroscopic characterization of the pulsed laser ablation plasmas for Cu, Al and Er^{3+}-doped Ti:$LiNbO_3$ targets is presented in Fig. 1 [3, 4]. The second harmonic (λ=532 nm) of a Q-switched Nd:YAG laser with 4.5 ns pulse duration, $0.1 \div 10$ Hz repetition frequency, was used for generating ablation plasma. The laser beam was focused on the target surface with a convergent lens with a focal f =20 cm and $N.A. = f/10$. The experiment was realized in air, at atmospheric pressure.

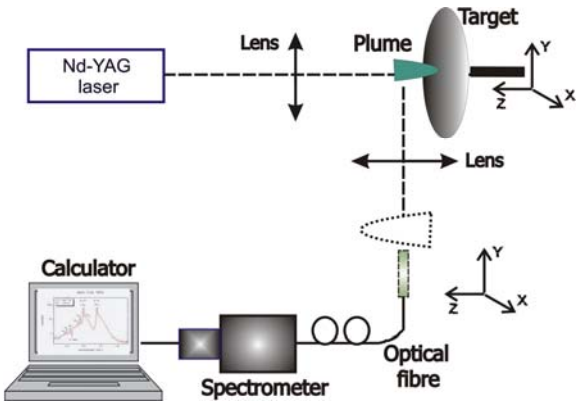

Fig. 1. The scheme of the experimental setup for emission plasma spectroscopy.

A plasma plume containing electrons, atoms and ions from the target and from the air was obtained. The plume dimensions are about 5 mm. The light emitted by the plasma was collected by an optical fiber-tip and carried at the entrance slit of an Acton Research spectrometer with 1200 grooves/mm blazed at 750 nm grating and a maximum resolution of approximatelly 0.5 nm. The spectrometer is used in the monochromator mode. Behind its exit slit, the light is detected by a Hamamatsu photomultiplier. For each wavelenght, the light intensity is integrated during at least a time equal with the inverse of repetition frequency of the laser shots. Then the light intensity is recorded by a computer. The computer controls also the grating rotation.

Some UV, visible and IR spectra of the Al (collected at several distances away from the target surface) and Cu plasmas obtained by pulsed laser ablation (10 Hz repetition frequency) are presented in Figs. 2 and 3, respectively.

The Al spectra (Fig. 2) give informations concerning the variation of the temperature along the axial direction of the plasma plume. The amplitudes of the maxima of the lines decrease with the distance from the target surface.

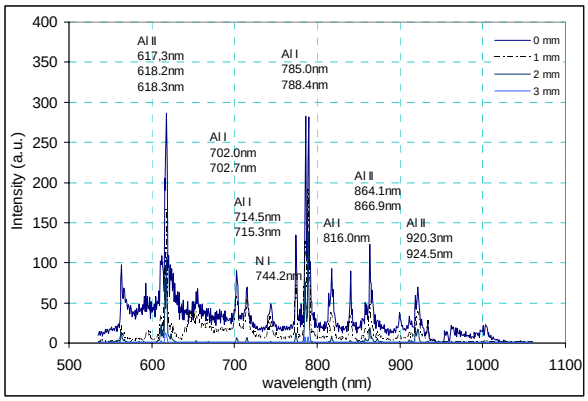

Fig. 2. Al plume spectra in visible and near-infrared regions at different heights above the target surface.

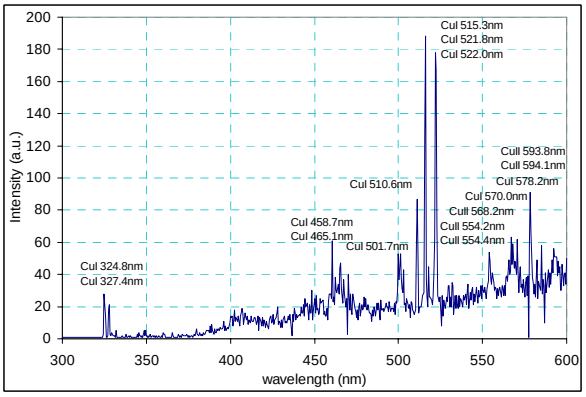

Fig. 3. Cu plume spectra in near UV and visible.

In the case of the ablation plasma generated on Cu, an expanded spectrum including the main lines in visible is presented in Fig. 4 a). It includes four atomic copper lines, separated by less than 12 nm (two being very closed near 521.9 nm). The profiles of the four Cu lines were fitted with Gaussian curve. Due to the very limited spectral resolution, the line profiles are given mainly by the

apparatus function of the measurement chain, which is Gaussian. For the spectral region of these four lines the spectral response is considered as constant. An energy calibration was not realized.

The emission coefficient is given by:

$$\varepsilon = \frac{1}{4\pi} n_u A_{ul} h\nu_0 \quad (1)$$

where ν_0 is the line frequency, n_u is the particle density in the upper level, A_{ul} is the emission rate for the spontaneous emission, and h is the Planck constant. Considering the plasma in local thermodynamic equilibrium (LTE), the Boltzmann distribution can be used to obtain the population in different excited levels, the expression of the emission coefficient being given by:

$$\varepsilon = \frac{n}{4\pi} \frac{g_u e^{-\frac{E_u}{kT}}}{Z(T)} A_{ul} h\nu_0 \quad (2)$$

where n is the total density of the considered species, g_u and E_u are the statistical weight and the energy of the upper level, and $Z(T)$ is the partition function.

The last expression is used in the following form:

$$I_k \sim \frac{N_{Cu}}{4\pi} \cdot \frac{g_{u,k}}{Z_{Cu}} e^{-\frac{E_{u,k}}{kT}} \cdot A_{ul,k} \frac{hc}{\lambda_k} \quad (3)$$

where the line intensity (in fact the light flux) was used instead the emission coefficient. Eq. (3) holds for optical thin plasmas, as we supposed implicitly, so that the intensity and light flux are strictly proportional. In Eq. (3) N_{Cu} represents the total number of the Cu species in the plume.

The electron (excitation) temperature is obtained from the slope $-\frac{1}{kT}$ of the best fit of the line:

$$\ln \frac{I_k \lambda_k}{g_{u,k} A_{ul,k}} = \ln \frac{hcN_{Cu}}{4\pi Z_{Cu}} - \frac{E_{u,k}}{kT} \quad (4)$$

in the plane with the energy E_u on horizontal axis and $\ln \frac{I\lambda}{g_u A_{ul}}$ on the vertical axis of the Boltzmann graph, as presented in Fig. 4 b. Considering the Cu plume spectrum presented in Fig. 4 a), with line intensities given by the surfaces of lines profiles, which lead to the Boltzmann's graph presented in Fig. 4 b, an electron temperature of about 7970 K is obtained for the Cu ablation plasma [4].

The effect of laser iradation on the target consists also in ablating the material with a certain rate Δh which gives the efficiency of pulsed laser ablation (PLA), representing the maximum depth of the ablated layer during the laser pulse:

$$\Delta h = h / N_p \ (\mu m / pulse) \quad (5)$$

where h represents the depth of the ablated crater and N_p is the number of laser pulses used to generate the desired structure. Fig. 5 a) presents the dependence of the crater depth on pulse number during percussion drilling of Er^{3+}-doped $Ti:LiNbO_3$ target in atmospheric air while Fig. 5 b) presents a 200 μm x 200 μm confocal microscopy image of a crater drilled by using 10 laser pulses at an intensity of 60 GW/cm^2 intensity.

The non-linear dependence of the crater depth on pulse number indicates that the ablation rate decays with pulse number. The decay could be associated with the trapping of the radiation and strong heating of the plume via inverse Bremsstrahlung into the deep craters that are drilled into the target when irradiating in multi-pulse regime.

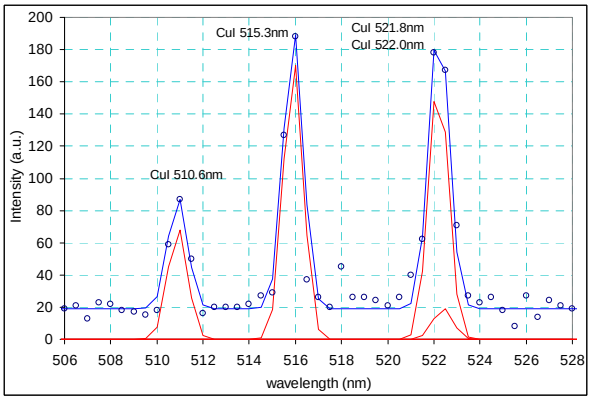

a)

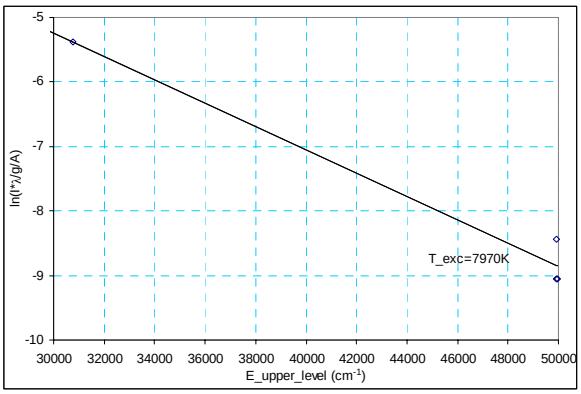

b)

Figs. 4 a), b). a) Cu plume experimental spectrum (small circles) and its fit using Gauss profiles. b) The Boltzmann's graph.

The non-localised heating of the whole crater-wall produced by the plasma plume rather than direct heating of the crater tip produced by the laser beam gives the non-linear dependence of the crater-depth and the decay of the ablation rate with pulse number.

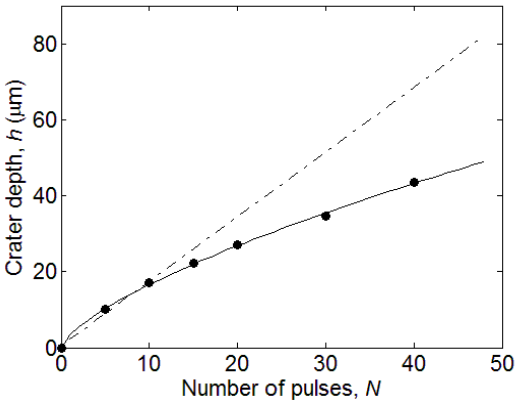

a)

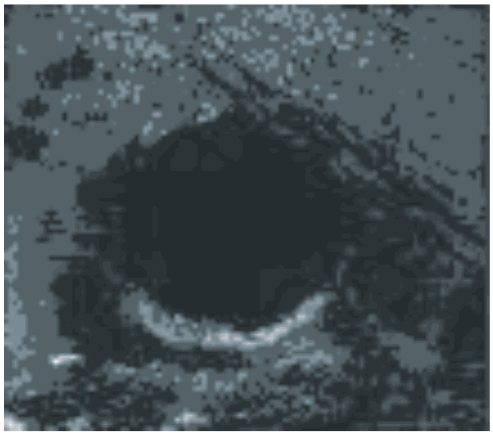

b)

Figs. 5 a), b). a) The crater depth vs. the pulse number. b) The confocal microscopy image of a crater drilled in $LiNbO_3$ target with 10 laser pulses.

The trapping of the plasma inside of the crater is demonstrated by the decay of the lines intensities that are reccorded at a fixed position above the target surface when increasing the number of consecutive pulses impinging the same spot on the target's surface. Part of the visible spectrum of the Er^{3+}-doped Ti:$LiNbO_3$ ablation plasma presenting the two main lines of neutral Li atoms at 610 and 671 nm is presented in Fig. 6 a)-c). Every point of the spectra was obtained by averaging the signal coming from maximum 10 consecutive laser pulses incident on the same spot, creating the condition of approximate constant ablation rate during this process.

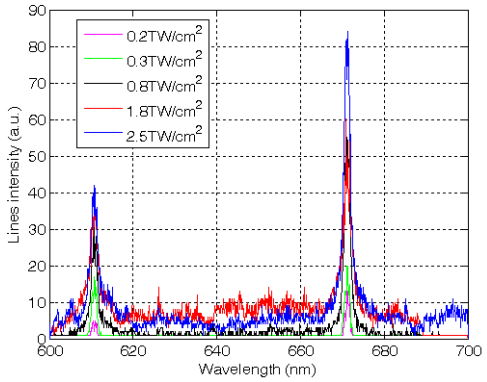

a)

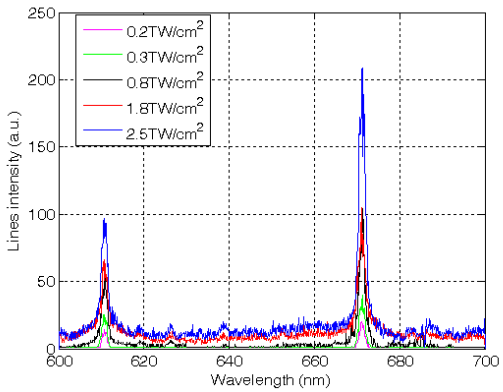

b)

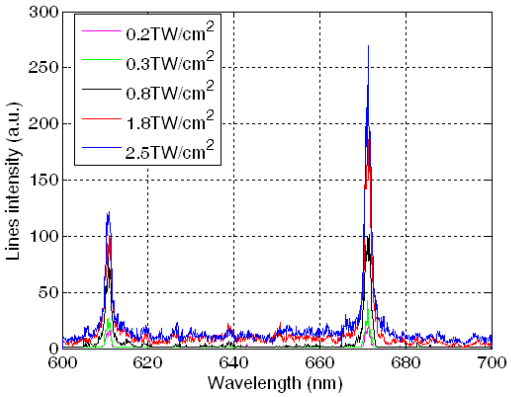

c)

Figs. 6 a)-c). The visible spectrum of the Er^{3+}:Ti:$LiNbO_3$ plasmas at different irradiances (in TW/cm^2) and different axial positions within the plasma plume: a) 0 mm, b) 1mm, c) 2 mm away from the target.

Increasing laser irradiance leads to the increase of the lines intensity whereas the ratio of the 671 to 610 nm lines intensities remains almost constant (~1.8) (Fig 7). When moving the observation point into the plume at larger distances (i.e. 1 and 2 mm away) from the target surface, the lines intensities obtained at a given laser irradiance become larger. These observations could suggest that the plasma is either richer in neutral Li atoms or hotter when increasing the laser irradiance and the distance from the target.

In order to decide what the case here is, the electron temperature was obtainted from the relative intensities of these atomic lines of Li I, at 610 and 671 nm, presented in Fig. 6. We took into account the Boltzmann's distribution of the atoms on the energetic levels for a thin plasma. The atomic data for these lines being given in Table 1[8].

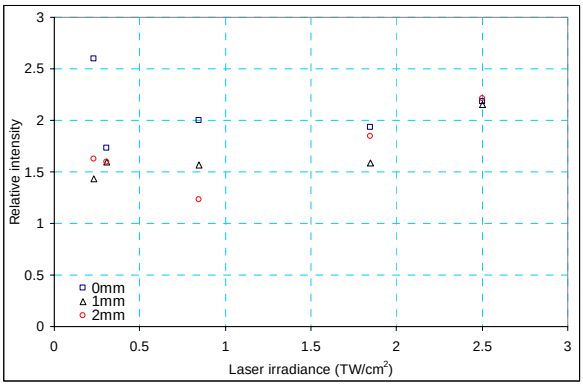

Fig. 7. The ratio of the 671 to 610 nm lines intensities vs laser irradiances at different axial positions within the plume of Er^{3+}:Ti:$LiNbO_3$ target as determines from the graphs presented in Fig. 6: near target (0 mm), 1 mm, and 2 mm away from target.

Due to a very limited spectral resolution of the measurement system, no line profile analysis was possible. So, no flattening of spectral profile in its center for homogeneous plasma and no absorption dip for a inhomogeneous plasma could be observed. But, due to the very probable self-absorption of the resonance lines radiation at 671 nm in the plasma, the emission coefficient corresponding to these lines is under-estimated. This fact leads to an estimated value of the electron temperature greater than the real value.

Table 1. Atomic data used for the treatment of Li I xperimental spectrum.

λ(nm)	$E_u\left(\text{cm}\right.$	J_u	$E_l\left(\text{cm}^{-1}\right)$	J_l	$A_{ul}\left(\text{s}^{-1}\right)$
610.35	31283	1.5	14899	0.5	$6.00\cdot10^7$
610.37	31283	1.5	14899	1.5	$1.20\cdot10^7$
610.37	31283	2.5	14899	1.5	$7.10\cdot10^7$
670.78	14904	1.5	0	0.5	$3.72\cdot10^7$
670.79	14904	0.5	0	0.5	$3.72\cdot10^7$

The results presented in Fig. 8 indicate that the plasma temperature as obtained from Li I lines is about 14000 K, being non-dependent on the laser irradiance or the position within the plume. Thereby, the difference in the lines intensities observed in Fig. 6 comes only from the richness in neutral Li atoms that are obtained at high laser irradiances. In fact, increasing laser irradiance leads to larger volumes and densities of ablated material rather than heating the plume.

3. Opto-acoustic methods

Optodynamics allows the study of the both thermal and optical effects induced by the laser radiation, such as the dynamics of the ablation products, ablation plasma, and the generation of shock waves during laser processing of a material [2, 9]. In this study we use a piezoelectric transducer (PZT) connected to a digital oscilloscope to determine the propagation time of the shockwaves through the target during the percussion drilling. The experimental setup is shown in Fig. 9 a). We used a "Brilliant" Q-switched Nd-YAG laser system provided with a second harmonic generator module (SHM).

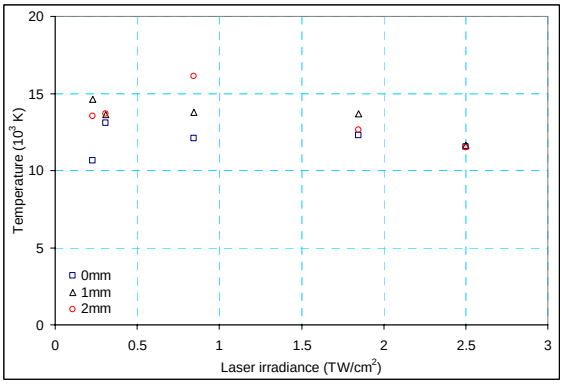

Fig. 8. Plasma temperature as a function of laser irradiance on an Er^{3+}:Ti:$LiNbO_3$ target for different positions within the plasma.

Laser pulses have 4.5 ns with 10 Hz repetition rate, with 360 mJ energy for the fundamental harmonic (1064 nm wavelength). The target was fixed in the lens focus to ensure a maximum irradiation at the target (Fig. 9 b)). Part of the scattered beam is detected by a photodiode (PD), whose signal triggers the time base of the oscilloscope. The signals from the PZT are digitally acquired on the oscilloscope and then processed and individually analyzed. A typical signal from the PZT during the drilling of a copper target is shown in Fig. 9 b). The shock wave propagating through the sample is a superposition of many waves originating from different points in the hole. For simplicity, here we consider that the shock wave originates from a point source at the bottom of the growing crater. With this assumption, the distance from the target surface to the origin of the shock wave is the hole depth h, while l is the distance from this origin to the rear target surface

where PZT is set (see Fig. 9 b). The first amplitude peak of the PZT signal was used to determine the propagation time *t* of the produced shock wave to the rear surface.

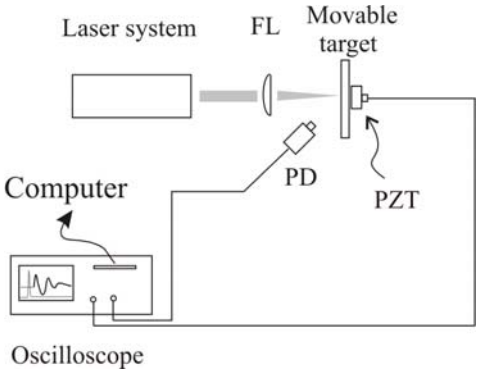

a)

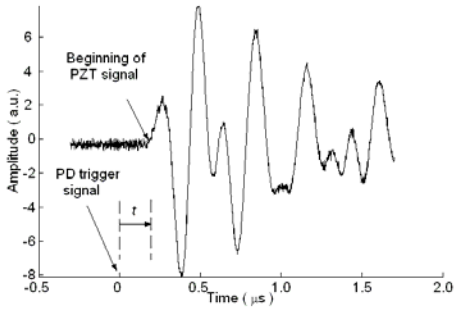

b)

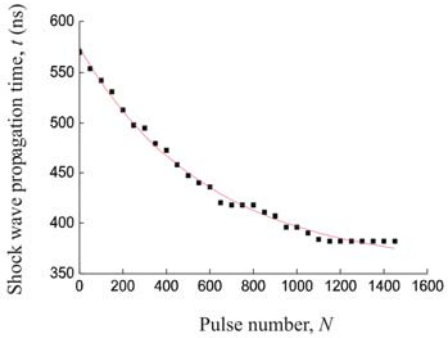

c)

Figs. 9 a)-c). Real-time determination and control of the laser drilled holes depth. a) Experimental setup for the etermination of the depth h of laser drilled holes. b) Determination of propagation time t of the shock waves within the target from a typical signal of the piezoelectric transducer. c) The dependence of the shock wave propagation time on the pulse number for a 2.5 mm thick coppertarget irradiated with 532 nm laser pulses.

In the early stages of the process, the distance l to the PZT and the propagation time t of the shock waves decreases strongly with the increasing the pulse number, resulting in an approximate exponential decrease of the ablation rate with pulse number. For a certain number of laser pulses (approximately 1000 for Al irradiated at 532 nm as indicated in Fig. 9 c), the shock-wave propagation time and hole depth cease to have an observable variation due to the less efficient transport of the ablation products out of the crater when the crater depth becomes comparable with the plasma hydrodynamic length. The number of pulses at which this change occurs is strongly dependent on the laser wavelength and on the optical and thermal properties of the material.

4. The TRR and RIP methods

The configuration of the experimental system and the samples preparation are outlined in details in papers [5-7]. The principles of TRR and RIP methods under hemispherical reactor are summarized in Fig. 10.

The sample is irradiated by an excimer KrF laser which emits light at a wavelength of 248 nm with a pulse duration of 27 ns (FWHM). The pulsed laser heats the sample and causes phase and morphological changes. Infrared radiations emitted from the surface of the sample are focused by two off-axis parabolic mirrors into the IR detector (liquid-nitrogen-cooled HgCdTe photodiode). The obtained signal (RIP signal) is then recorded on a digital oscilloscope (500 MHz). In order to obtain the absolute surface temperature, the IR detector's output is calibrated for each sample [6].

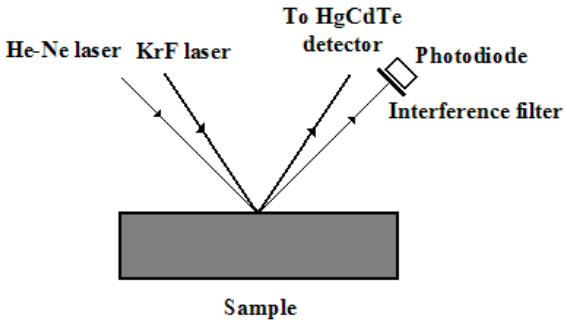

Fig. 10. The schema of TRR and RIP methods.

The TRR method is used to study phase transitions on the sample's surface during and after the KrF laser irradiation. Since the reflectivity coefficient (of Au in our case [6]) has high values in the red and IR band, we used a 10 mW CW He-Ne laser beam at 632.8 nm for probing. The red light is precisely directed and focused into the central part of the heated zone of the sample and forms a spot, one order of magnitude smaller than the heated area. The reflected light is detected with the photodiode and amplified using a variable gain high-speed voltage amplifier. The heating laser beam is first homogenized in

order to achieve a uniform thermal field that gives good results within rapid pyro/reflectometry methods. In order to study several materials with different melting and ablation thresholds, the KrF fluence (energy/surface) is varied from 100 to 2000 mJ/cm^2. In this paper we investigated the metallic thin film (Au/Ni).

Melting is clearly shown in both TRR and RIP signals that translate the typical thermodynamic behaviour of thin films irradiated by low laser fluences (less than 500 mJ/cm^2). In the case of Ti surface, the results presented in paper [6] show two distinguished regimes: the first one, bellow 1000 mJ/cm^2, corresponding to the early stage plasma initiation, and the second one, over 1000 mJ/cm^2, corresponding to the dynamics of expanding plasma.

For metals, in the frequency (ω) range of the used lasers, when the plasma frequency $\omega_p << \omega$, the reflectivity coefficient, R is given by the equation [6]:

$$R = 1 - \frac{4\omega\varepsilon_0}{\sigma c} \tag{6}$$

where σ is the electric conductivity, ε_0 is the dielectric constant of the vacuum and c is the speed of light in vacuum.

The probe laser is reflected not only at the sample surface but penetrates it on a certain depth, named optical penetration depth. When the sample is irradiated by the pulsed laser the material melts on a certain depth, δ_m. In the case $\delta_m << \delta$ the probe laser radiation is reflected by the both liquid and solid phases.

The target reflectivity depends on the temperature and the phase variations of the sample's surface during the melting process. It changes from the value R_s which characterizes the solid phase to a higher value R_l which characterizes the liquid phase. R_l remains constant during the time of melting t_m which is longer than the laser pulse duration. After being heated, the surface of the sample is cooled again; this causes the resolidification of the material and, consequently, the decrease of the reflectivity. If the obtained film is monocrystalline, then the values of R_l and R_s are the same ($R_l = R_s$); if it's not ($R_l \neq R_s$), then it's the case of imperfect recrystallization.

The Au/Ni/Bronze conductivity spectrum evaluated using Eq. 6, for several values of laser fluence, is presented in Fig. 11. As can be seen, the conductivity curve has the same behaviour as the reflectivity one. The range of deduced electrical conductivity is in a good agreement with databases for gold surfaces.

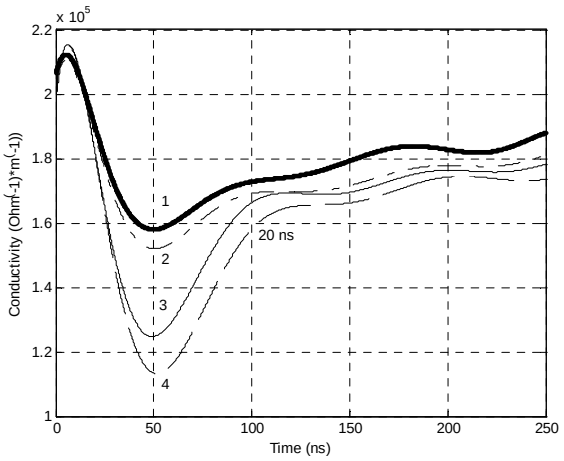

Fig. 11. The computed conductivity spectrum in the case of Au/Ni/Bronze for laser fluences of 515 mJ/cm^2 (curve 1), 644 mJ/cm^2 (curve 2), 902 mJ/cm^2 (curve 3) and 1031 mJ/cm^2 (curve 4).

This material (Au/Ni/Bronze) was rarely investigated by the time resolved pyro/reflectometry because of the complex phenomena behind this laser-material interaction [6, 7]. After the electro-deposition and the laser surface treatment, they are used in electrical contact applications. The laser surface treatment is used because it suppresses the porosity and smoothness of the surface, allowing a good electrical contact [7].

Using the calibration curves presented in paper [10], we computed the temperature dependence of the electric conductivity in the case of Au/Ni/Bronze vs. temperature for laser fluences of 1031 mJ/cm^2 and 902 mJ/cm^2, in the temperature range of 300-700 K (Fig. 13). As can be seen from Fig. 12, the electric conductivity of Au/Ni/Bronze coating decreases with the temperature following a parabola.

Taking into account the model presented in paper [9] for the above mentioned conditions, we evaluated the time dependence of the apparent (non-uniform) effusivity after the absorption of a Dirac pulse with the density of energy Q:

$$e_{app}(t) = \frac{Q}{T(t)\sqrt{\pi t}} \tag{7}$$

where $T(t)$ represents the time dependence of the surface temperature of the semi-infinite material (Fig. 13 a). Also, in order to eliminate the effect of the finite pulse duration, τ we used a more general equation to evaluate the effusivity [9] (Fig. 13 b):

$$e^*(t) = \frac{2Q}{T(t)\tau\sqrt{\pi}}\left(\sqrt{t} - \sqrt{t-\tau}\right), \text{ for } t > \tau. \tag{8}$$

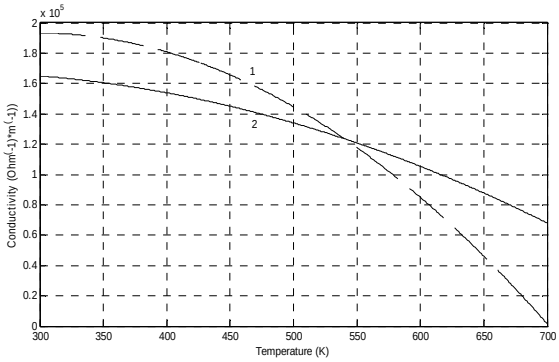

Fig. 12. The computed conductivity in the case of Au/Ni/Bronze vs. temperature forlaser fluences of 1031 mJ/cm^2 (curve 1) and 902 mJ/cm^2 (curve 2).

As can be seen from Figs. 13 a)-b), the effusivity decrease in time for both laser fluences to that corresponding for Au, of about ~28600 $Ws^{1/2}m^{-2}K^{-1}$ (curves 1) [9].

5. Conclusions

In this paper we studied the Al, Cu, and Er^{3+}-doped $Ti:LiNbO_3$ ablation plasmas under room conditions using spectroscopic methods. We obtained the UV, visible and IR spectra of the laser-ablation plasmas of the above mentioned specimens. Using the visible spectrum, we evaluated the temperature of several Cu ablation plasmas. The obtained results are in good agreement with other published in the literature [1, 2] and may be used for the evaluation of plasma parameters such as temperature, electron density.

The laser-ablation plasmas and the generated shock waves generated in multi-pulse regime were further characterized by using an opto-acoustic method. The results indicated a decrease of the ablation rate of the metallic (Al) target due to the enhanced laser-plasma interaction when plasma becomes trapped into the deep crater.

We used the TRR and RIP methods to study the phase transitions on the Au/Ni/Bronze coating surface during and after laser irradiation and also to evaluate the conductivity spectrum for several values of laser fluence. As can be seen, the conductivity curve has the same behavior as the reflectivity one [6]. We found that in the temperature range 300-700 K the electric conductivity of Au/Ni/Bronze coating decreases with the temperature following a parabola. Also, we found that the computed effusivity decrease in time in the interval 30-70 ns for both laser fluences, 1031 mJ/cm^2 and 902 mJ/cm^2, respectively to that corresponding for Au of about ~28600 $Ws^{1/2}m^{-2}K^{-1}$.

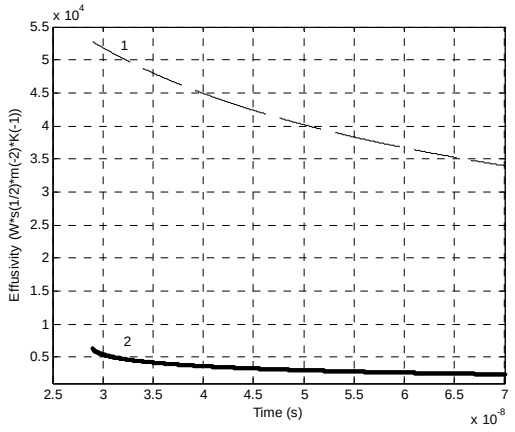

a)

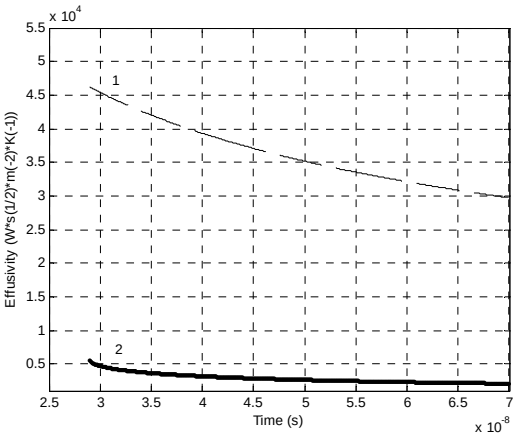

b)

Figs. 13 a), b). The effusivity of Au/Ni/Bronze vs. time in the case of a pulse duration τ = 27 ns for laser fluences of 1031 mJ/cm^2 a) and 902 mJ/cm^2 b), curve 1 representing the apparent effusivity and curve 2 the effusivity obtained using the general equation.

References

[1] S. Amoruso, R. Bruzzese, N. Spinelli, R. Velotta, J. Phys. B: At. Mol. Opt. Phys., **32**, 131 (1999).
[2] I. Pauleau, Laser Beam-Solid Interactions: Fundamental Aspects, Elsevier, (2005).
[3] S. S. Ciobanu, C. Negutu, M. Stafe, I. Vladoiu, V. Pais, V. Stancalie, N. N. Puscas, 35th EPS Conference on Plasma Phys. Hersonissos, 9 - 13 June 2008, ECA, **32D**, 5,144 (2008).
[4] C. Negutu, M. Stafe, S. S. Ciobanu, I. Vladoiu, N. N. Puscas, University "Politehnica" of Bucharest, Sci. Bull., Series A: Applied Mathematics and Physics, **70**(3), 85 (2008).

[5] J. Martan, O. Cibulka, N. Semmar, Appl. Surf. Sci., **253**, 1170 (2006).
[6] N. Semmar, M. Tebib, J. Tesar, N. N. Puscas, E. Amin-Chalhoub, Appl. Surf. Sci., **255,** 554 (2009).
[7] C. Georges, N. Semmar, C. Boulmer-Leborgne, Optics and Lasers in Engineering, **44**, 1283 (2006).
[8] J. Reader, C. H. Corliss, W L. Wiese, G. A. Martin, Wavelengths and Transition Probabilities for Atoms and Atomic Ions Part 1. Wavelengths, Part 2. Transition Probabilities, NSRDS-NBS **68**, 415 (1980).
[9] J. Martan, N. Semmar, C. Leborgne, E. Le Menn, J. Mathias, Appl. Surf. Sci., **247**, 57, (2005).
[10] M. Stafe, C. Negutu, I.M. Popescu, Shock Waves, **14**, 123 (2005).

*Corresponding author: pnt@physics.pub.ro